Assessment of the influence of the bending form shape on the stress and plastic strain values in a cold bending pipe

Krzysztof Nozdrzykowski[1], Mateusz Stępień[2], Zenon Grządziel[3]

[1] https://orcid.org/0000-0003-2785-0868
[2] https://orcid.org/0009-0009-8986-1643
[3] https://orcid.org/0000-0001-9348-1111

[1,3] Maritime University of Szczecin, Faculty of Marine Engineering
2 Willowa St., 71-650 Szczecin, Poland
[2] Piping Company 'Chemar Rurociągi' Sp. z o. o., Kielce, Poland
e-mail: [1]k.nozdrzykowski@pm.szczecin.pl
corresponding author

Abstract
This paper presents the results of modelling research concerned with the technological process of the cold bending of a pipe. Stress and plastic strain studies are carried out using the finite element method (FEM) on a thick-walled pipe and various shapes of bending form. The results of the research are benchmarked in terms of the correctness of the implementation of the bending process, including the change in the pipe outside diameter and wall thickness. The level of ovalisation of the cross-section in the bending pipe is used as the primary criterion for assessing the correctness of the bending process. The results show that the most favourable properties in terms of minimising the ovalisation of the pipe cross-section are provided by the use of a bending form with a trapezoidal shape.

Introduction

In many industrial sectors, the energy medium is transported by pipelines and all the necessary equipment. Examples of this type of industry include power stations, gas pipelines or energy from waste plants (waste incineration). Pipelines are an important and necessary part of the maritime industry in the broadest sense and of related industries such as shipbuilding (Jóźwiak, 2011; Młynarczak, 2013). The pipeline route is designed according to the technologist's guidelines. However, the route is often adapted to the secondary structure (i.e., the ceilings, beams and floors). This is why there are both straight and bending pipes along the pipeline route. Pipelines are, therefore, assembled from straight and bending pipes and various

components such as fittings, flanges, valves, gate valves, orifices, expansion joints, shock absorbers, etc. The process of bending pipes prefabrication is particularly interesting from the point of view of the production process realisation of the mentioned elements. Bending pipe could be produced in two ways: by cold bending and induction bending. In the process of cold bending, commonly called mechanical, the basic elements, besides the formed pipe, are the rotating bending form, clamping die, and pressure die, as shown in Figure 1 (Trzepieciński, 2016; Packer, 2018; Płonecki, Witkowski & Kurp, 2018; Traczyk, 2019; Thomas, 2020).

The device used for the cold bending process is called a bending machine, an example of which is shown in Figure 2.
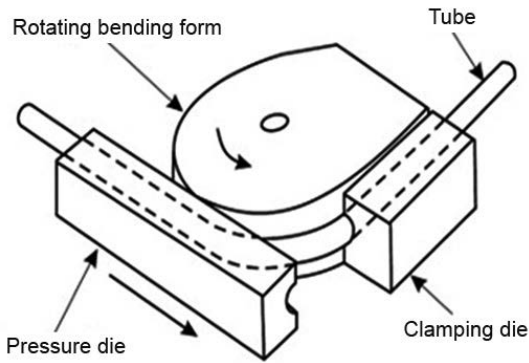
Figure 1. Cold bending process diagram (Packer, 2018)

During the bending process, the cross-section is ovalised with a simultaneous change in the wall thickness at the circumference of the pipe (Fukuda et al., 2002; Fukuda et al., 2003; Horikawa & Nobuhisa, 2009; Sen, Cheng & Zhou, 2010). The bending process is also accompanied by an increase in the von Mises stress present in the bending pipe, which necessitates the application of an appropriate heat treatment (annealing), after finishing the bending process. Cross-section changes disrupt the flow of media, and the cleaning and maintenance processes required to maintain proper exploitation are more difficult to perform. These changes also contribute to a reduction in the strength of the bending pipe in the tension zone, where the phenomenon of pipe wall thickness decrease occurs. Furthermore, a greater ovalisation causes an increased error

Figure 2. Cold bending machine

in calculating the stresses in the pipeline. In a perfectly circular cross-section, there is a different pressure distribution than in an element with an elliptical outline. Therefore, bending pipe sections are subject to the assessment of their dimensional and shape performance in accordance with applicable standards. For the energy industry, the applicable standard in this area is, for example, EN 13480 (PN-EN 13480:2021). It defines the allowable corrugation in the compression zone, the maximum allowable ovalisation and the minimum wall thickness in the tension zone.

Depending on the operating conditions in which the manufactured components operate, the material

Table 1. Typical materials and their mechanical properties used for piping components, distinguishing between selected industrial sectors

Material grade	Application				Mechanical properties					
	Conventional power plant	Gas pipelines	Waste incineration	Ship-building	R_e [MPa] [*]$T \le 16$	R_m [MPa]	A [%]		KV [J] in temp. +20 °C	
							[**]l	[***]t	[**]l	[***]t
X10CrWMoVNb9-2 (P92)	+				440	620–850	19	17	40	27
X10CrMoVNb9-1 (P91)	+			+	450	630–830	19	17	40	27
10CrMo9-10	+		+	+	280	480–630	22	20	40	27
15NiCuMoNb5-6-4 (WB36)	+				440	610–780	19	17	40	27
13CrMo4-5	+		+		290	440–590	22	20	40	27
16Mo3	+		+	+	280	450–600	22	20	40	27
X6CrNiMoTi17-12-2	+		+		210	500–730	35	30	100	60
L555MB		+			555	625–750	24	18	60	40
L415NE		+			415	520–760	20	18	60	40
34CrMo4	+			+	800	1000–1200	16	11	40	27
P265GH	+		+	+	265	410–570	23	21	40	27
25CrMo4	+			+	345	540–690	18	15	40	27
14MoV6-3	+				320	460–610	20	18	40	27

[*]T – pipe wall thickness, [**]l – longitudinal direction, [***]t – transversal direction.

used should be selected accordingly. Table 1 provides an overview of the materials used for piping components in the previously mentioned industries (Adamiec & Dziubiński, 2000; Sen et al., 2006; Euro Inox, 2007; Szewczyk, 2017).

As mentioned earlier, an important issue occurring during the shaping of a bending pipe is the ovalisation of the cross-section and the variation of the wall thickness in the radial direction. The issue of the influence of the shape of the bending form on the geometric condition of the bend is treated marginally in the available literature. Observations made during the pipeline process improvement work suggested that the shape of the bending form profile may have a significant impact on the geometric condition and stress values of the bending pipe. These suggestions led the authors to carry out such a study. The results are presented in this article.

Investigated object

The assumed framework research plan predicted analysis of plastic strain and von Mises stress occurring during the shaping of a piping element using a bending form with circular, oval and trapezoidal shapes. The next stage in the assumed research plan was to find the ovalisation level in the pipe cross-section and the thinning and thickening of their wall thickness. The next stage in the adopted test plan was to determine the level of ovalisation in the designated cross-section of the pipe and the thinning and thickening of the pipe wall. The research was carried out on a thick-walled pipe, which means that the outer-to-inner diameter ratio is greater than 1.7. Calculations were carried out using the finite element method (FEM) with extensive simulation capabilities (Damslet et al., 1999; Niezgoda, Małachowski & Szymczyk, 2004; Kenedi, Borges & Vaz, 2008; Riagusoff et al., 2010; Sen & Cheng, 2010; Domanowski & Nowak, 2011; Cakiroglu et al., 2014; Xinwei et al., 2021). It should be noted that the available reference materials also describe the principles for determining stresses and strains in bending pipe using analytical methods (Śloderbach, 1998; Śloderbach & Kaźmierczak, 2001; Serebrennikov & Serebrennikov, 2018).

The simulation was performed using ANSYS 2019 and the newer version, ANSYS 2022 (Simu Tech Group, 2019). The bending process was modelled according to the diagram shown in Figure 1. The geometric model adopted for the analysis is shown in Figure 3. In subsequent modelling steps, only the shape of the bending form was changed.
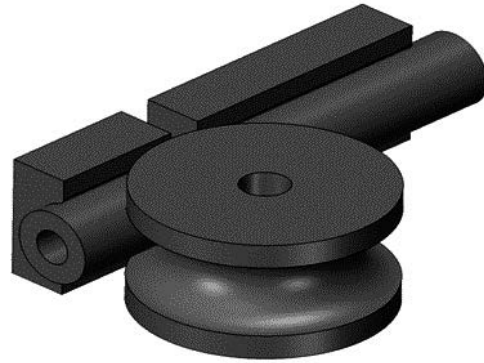

Figure 3. Geometrical model of the bending form and dies

The test object was a pipe of 12 mm diameter and 3.2 mm wall thickness. The initial assumption was that the bending radius would be 18 mm. The assumed small dimensions of the elements were related to the number of finite elements that formed the discretised numerical model. The simulations carried out were difficult in terms of achieving model convergence during successive iterations of the non-linear analysis and required the use of a high-quality mesh, which caused a very long calculation time. The material model adopted for the pipe for the analysis was a default non-linear stainless steel model with a yield strength of 210 MPa, Young's modulus of 193 GPa, density of 7.75×10^3 kg/m^3 and Poisson's ratio of 0.31. The material model assumed for the study was an elasto-plastic model, which is presented in Figure 4.
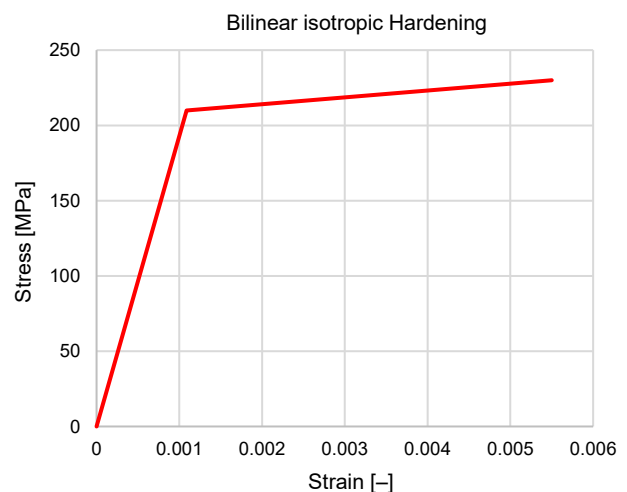

Figure 4. Material model adopted for the study

For the remaining components (the bending form and the two dies), a default linear material model, defined in ANSYS as 'structural steel', was adopted.

The material had the following properties: Young's modulus of 200 GPa, Poisson's ratio of 0.3 and density of 7.85×10^3 kg/m^3. It was assumed that

no plastic deformation would occur in these model components (the bending form and the two dies), so the von Mises stress values exceeding the applicability of Hooke's law, requiring the use of a non-linear material, were not expected. The boundary conditions adopted in the analysis are presented in Figures 5(a), (b) and (c).

The analysis assumed rotation of the clamping die around the local coordinate system, which was determined in the hole of the bending form (Figure 5(a)). Another assumption was to rotate the bending form around the same axis as the clamping die

(Figure 5(b)) and fix the displacement of the clamping die (Figure 5(c)). Before starting the simulation, the mesh quality parameters were checked (Element Quality Plots in Ansys Workbench, 2019 R2). Figure 6 shows one of the most important parameters representing the quality of the individual mesh elements in the analysed geometry, which was the element quality. When checking the quality parameters of the mesh, the authors focused only on the pipe section because it was the most important body in the study. Hence, the quantity of the mesh finite elements was increased only in the contact zones.
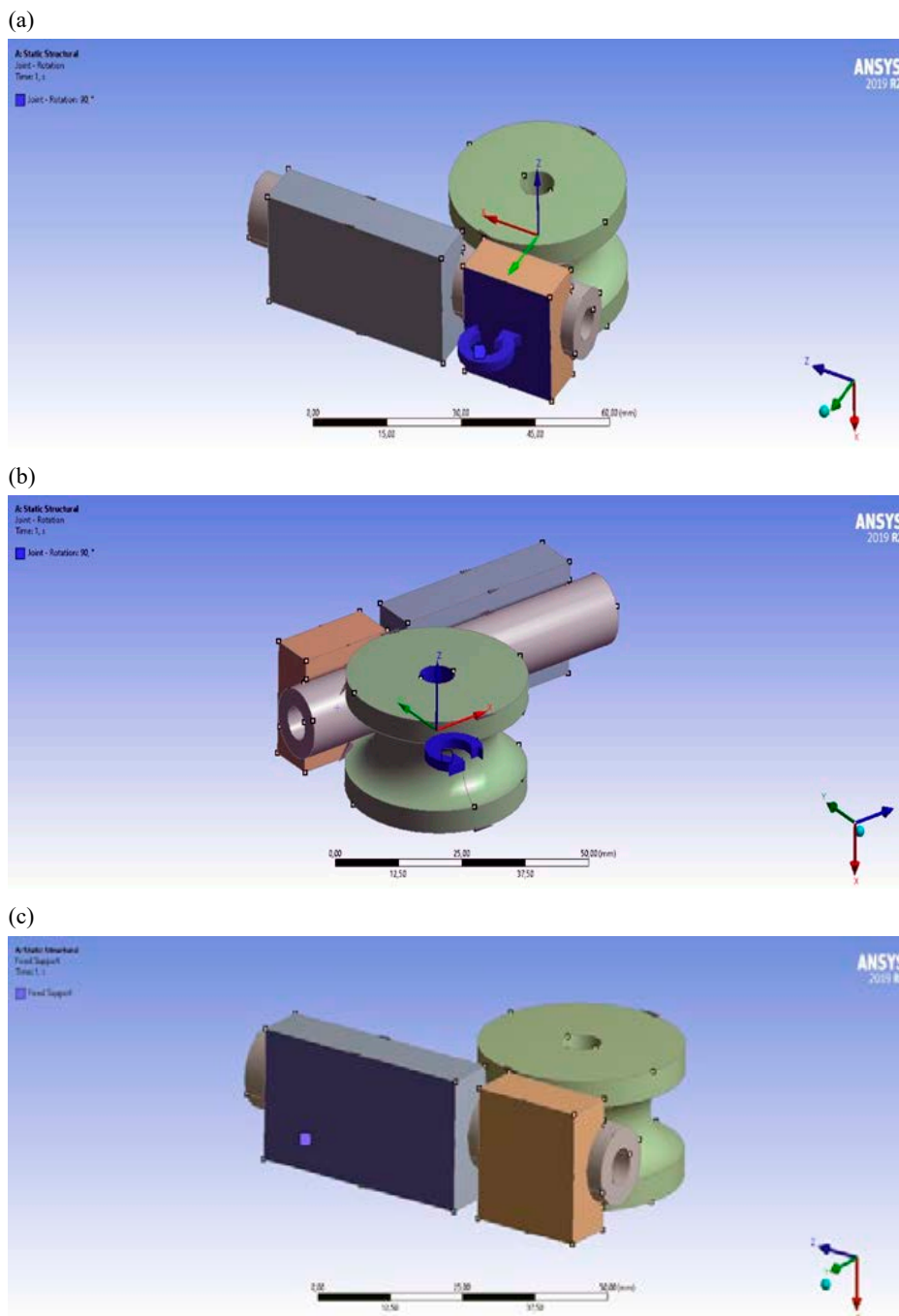
(a)

(b)

(c)

Figure 5. Boundary conditions used in the analysis: (a) clamping die rotation, (b) bending form rotation, (c) fixed pressure die
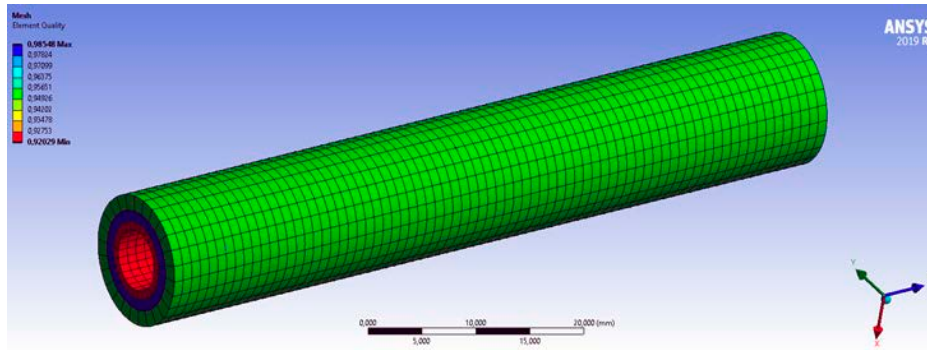
Figure. 6. One of the mesh quality parameter – quality element

Table 2 presents the verified mesh quality parameters. Based on the results, it can be concluded that the modelled mesh was of very good quality.

Table 2. Mesh quality parameters

Parameter	Perfect value	Bad mesh quality	Worst value in the pipe
Element quality	1	0	0.9
Aspect ratio	1	over 20	1.48
Jacobian ratio	1	over 30	1.36
Warping factor	0	over 1/0.4	1.49×10^{-13}
Parallel deviation	0	170	14.77
Maximum corner angle	60°/90°	aiming at: 165°/180°	98.5
Skewness	0	1	0.096

The finite elements used are Hex20, which are solid hexagonal finite elements consisting of 20 nodes.

The analysis of the first bending form, with a circular profile, included four components with a total of 28,814 finite elements, connected by 69,130 nodes. The geometric model is presented in Figure 7.

The analysis results for the first considered bending form shape are shown in Figures 8–10.

Figure 8(a) shows the distribution of the von Mises stress presented in a side view. Figure 8(b) displays the distribution of the von Mises stress in the cross-section of a bending pipe using a bending form with a circular profile. In Figure 9, the distribution of the von Mises stress occurring in the outer tensile layer of the bending pipe (Figure 9(a)) and the inner compression layer of the bending pipe (Figure 9(b)) are presented.

The simulation was carried out according to the assumption that the investigated object will be a bending pipe with a bending radius of 18 mm and a bending angle equal to 90°. The different stress values in the two layers show that the model behaves according to the knowledge of the strength of materials in the context of bending a curved bar. This is because, in this case, the neutral axis has moved to the axis of curvature. In the last iteration of the bend-bending simulation, the maximum value of the von Mises stress reached 783 MPa. Figure 10 shows the distribution of plastic deformation occurring in the outer tensile layer of a bending pipe (Figure 10(a)) and the inner compressive layer of a bending pipe (Figure 10(b)). The maximum plastic strain value reached 31.2 %.

After the simulation, the values obtained had to be analysed in detail to ensure that they were correct and according to the expectations and engineering intuition. Values close to 783 MPa correspond
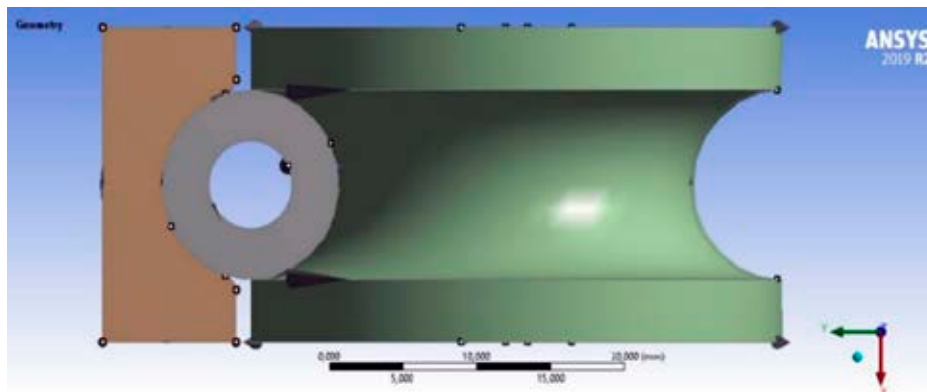

Figure 7. Geometrical model of the first investigated case - circular bending form
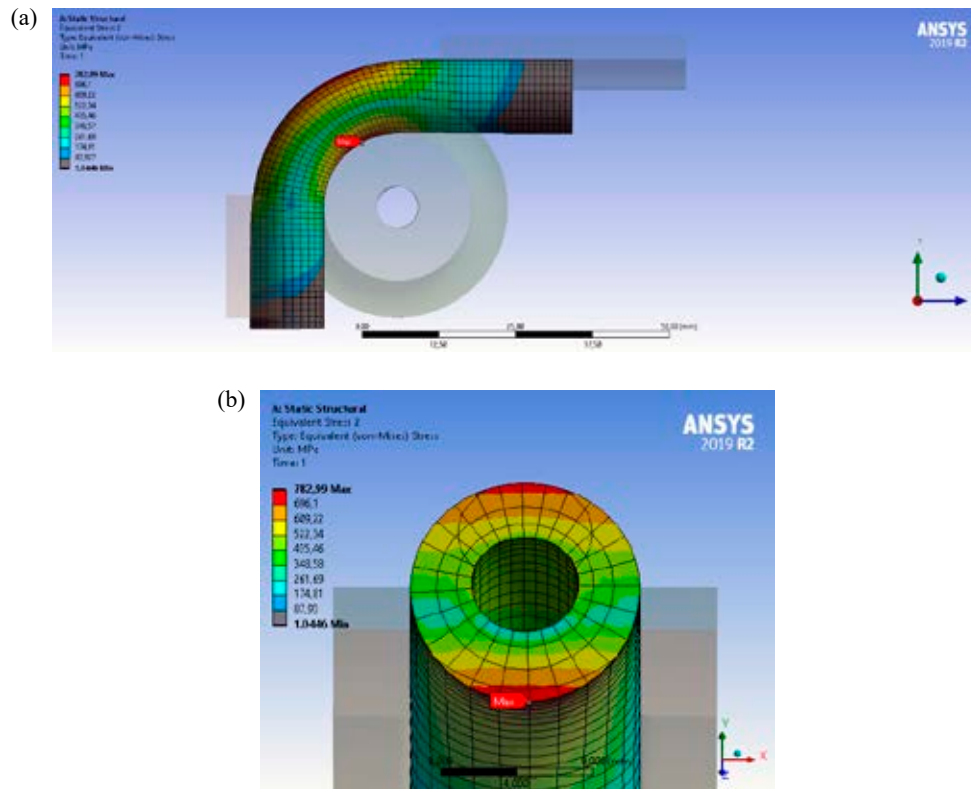
Figure 8. (a) Side view of the Von Mises stress distribution in a bend and (b) circular profile bending form of the von Mises stress distribution in the cross-section of a bending pipe
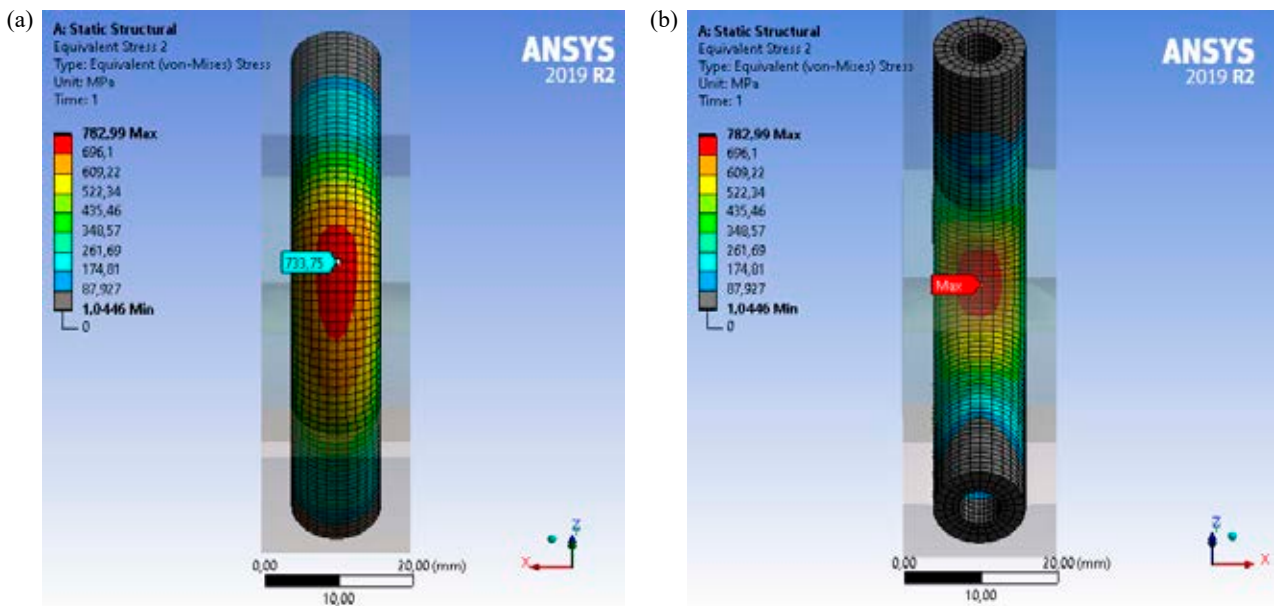

Figure 9. Distribution of the von Mises stress occurring in the (a) outer tensile layer of the bending pipe and (b) inner compression layer of a bending pipe

to a plastic strain of 31.2 %. The question to be answered here is whether such high values for the parameters presented are realistic. In the analysis carried out, the material was assumed to be stainless steel. Austenitic stainless steels with a yield point of about 200–230 MPa are characterised by a high

value of the A parameter, which means the plastic deformation at its breakpoint (i.e., elongation at break) (Euro Inox, 2007). Hence, it can be assumed that the obtained results are correct.

The second stage of the study was to analyse the strain and stress during the forming of the pipe
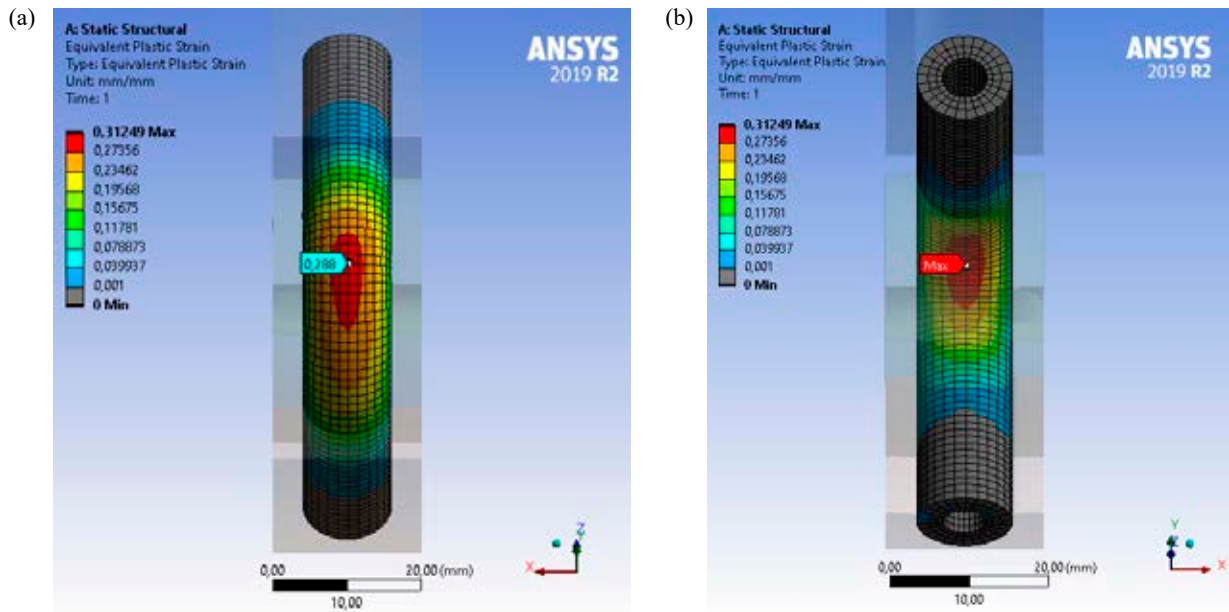
(a)

(b)

Figure 10. Distribution of plastic strain occurring in the (a) outer tensile layer of a bending pipe and (b) inner compression layer of a bending pipe
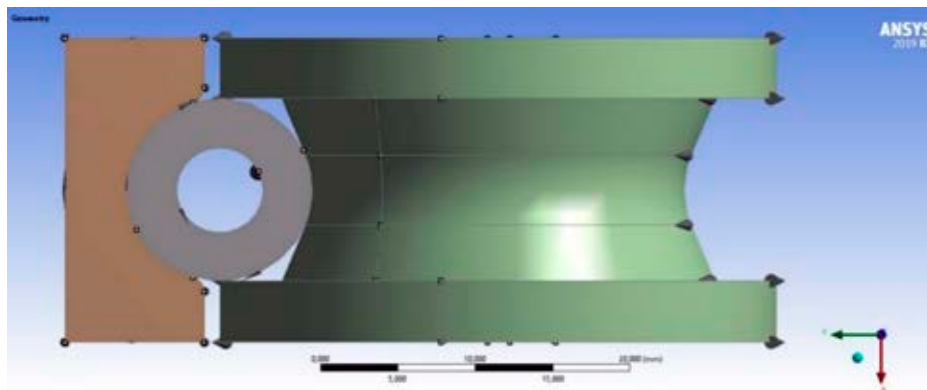

Figure 11. Geometrical model of the second investigated case – oval bending form

using a bending form with an oval profile. In adopting the shape shown in Figure 11, the authors were guided by the need to reduce the contact area and not limit the deformation in the upper and lower zones of the pipe. The study, therefore, did not consider the contact between the pipe and the top and bottom surfaces of the bending form (where the bending form has the largest diameter in the Z-Y plane).

The results of the analysis for the second considered bending form shape are shown in Figures 12–14.

Figure 12(a) shows the distribution of the von Mises stress presented in a side view. Figure 12(b) shows the distribution of the von Mises stress in the cross-section of a bending pipe using a bending form with an oval profile. In Figure 13, the distribution of the von Mises stress occurring in the outer tensile layer of the bending pipe (Figure 13(a))

and the inner compression layer of the bending pipe (Figure 13(b)) are presented.

When analysing the results obtained after simulating the bending of the pipe using the bending form shape shown in Figure 11, it can be observed that the von Mises stress values are slightly higher compared to the results from the first analysis. In the described case, the maximum von Mises stress value reaches 791 MPa.

A comparison of the results with the first analysis also shows higher plastic deformation values. In the described case, the maximum value of plastic strain reaches 31.5 %. However, more deformation can be visually observed in the deformed model, as highlighted in Figure 14, which shows the distribution of plastic deformation occurring in the outer tensile layer of the bending pipe (Figure 14(a)) and the inner compression layer of the bending pipe (Figure 14(b)).
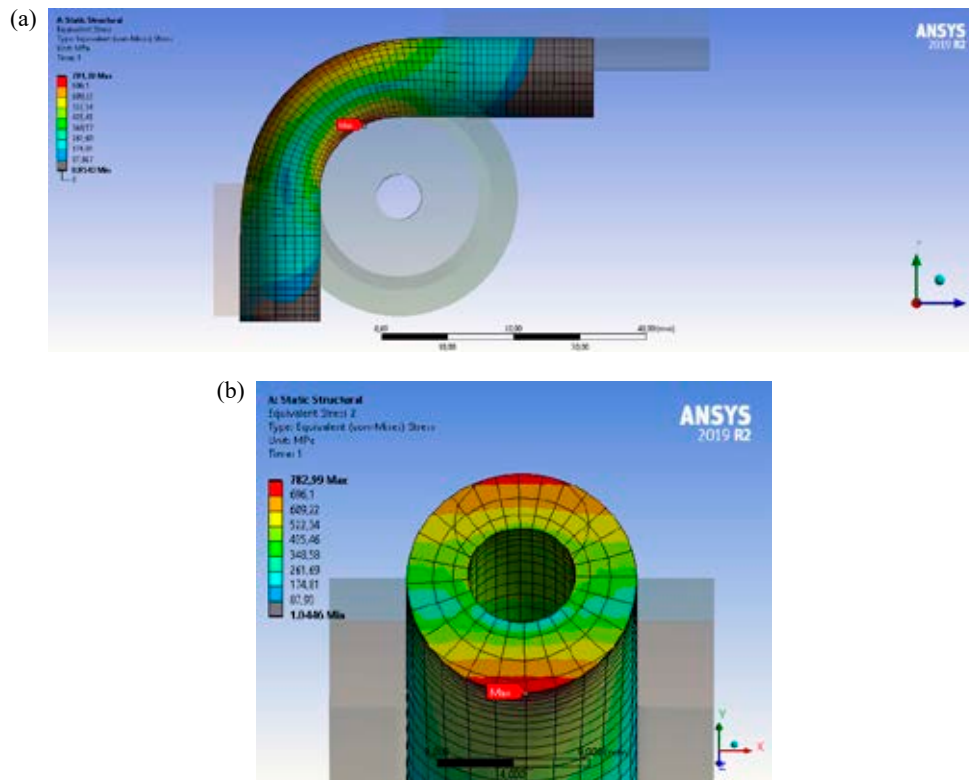
Figure 12. (a) Side view of the Von Mises stress distribution in a bend and (b) oval profile bending form of the von Mises stress distribution in the cross-section of a bending pipe
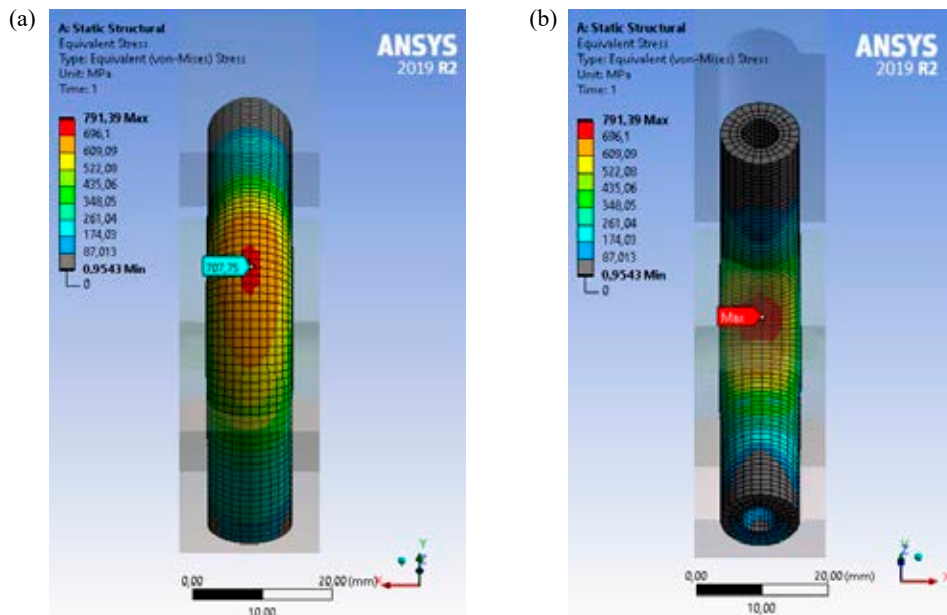

Figure 13. Distribution of the von Mises stress occurring in the (a) outer tensile layer of the bending pipe and (b) inner compression layer of a bending pipe

The third stage of the adopted research plan involved the analysis of stress and strain during pipe forming using a bending form with a trapezoidal profile, as illustrated in Figure 15. When selecting the presented shape, the authors were guided by assumptions opposite to those presented for the second analysis. In the described approach, the shape

was chosen to minimise the contact areas by limiting themselves to the top and bottom zones of the bending form only.

The results of the analysis for the third considered bending form shape are shown in Figures 16–18.

Similar to previously, Figure 16(a) presents the von Mises distribution in a side view. Figure
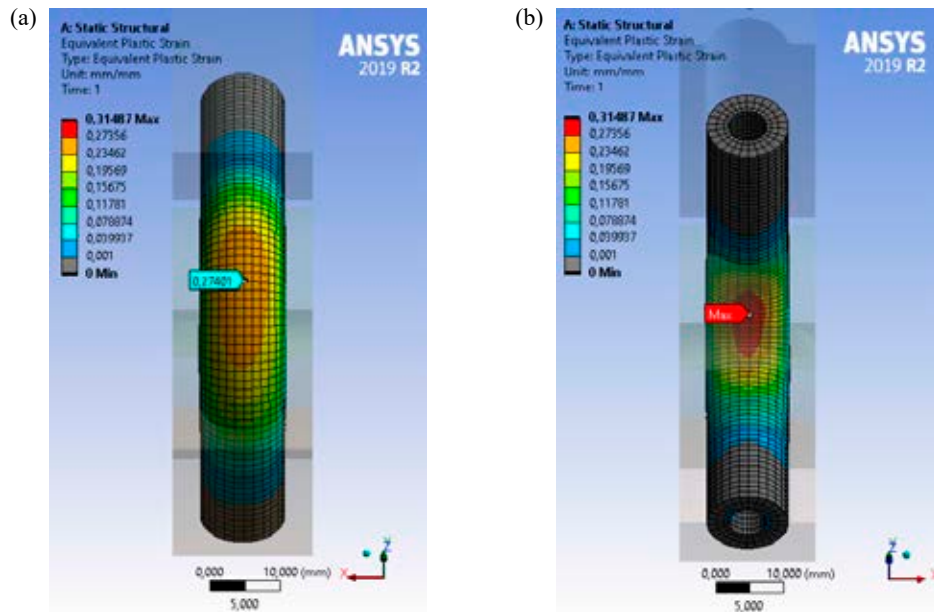
Figure 14. Distribution of the plastic strain occurring in the (a) outer tensile layer of a bending pipe and (b) inner compression layer of a bending pipe
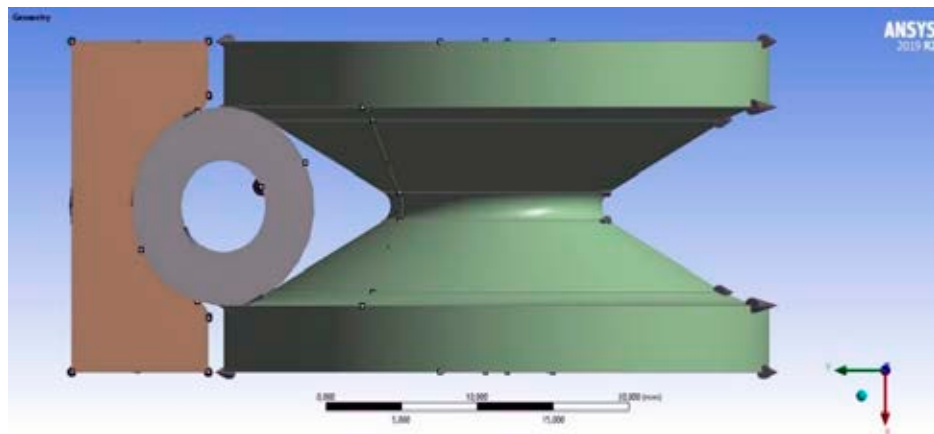

Figure 15. Geometrical model of the second investigated case – trapezoidal bending form

16(b) shows the distribution of the von Mises stress in the cross-section of a bending pipe using a bending form with a trapezoidal profile. In Figure 17, the distribution of the von Mises stress occurring in the outer tensile layer of the bending pipe (Figure 17(a)) and the inner compression layer of the bending pipe (Figure 17(b)) are presented.

The results obtained are greater than those obtained in previous studies. However, visually, it can be observed that there is less deformation in the currently analysed geometry. The maximum value of the von Mises stress is equal to 813 MPa.

Plastic strain in the third case achieves 33 %. The plastic strain distribution occurring in the outer tensile layer and inner compressive layer of the bend is presented in Figures 18(a) and 18(b), respectively. The presented values are within the range in which, according to the assumed mechanical properties

of the material model, the crack in the pipe will not become a problem.

Table 3 provides a summary of the results of the von Mises stress and plastic strain in the compression and tensile layers for the bending form shapes that were analysed.

Table 3. Comparison of the von Mises stress and plastic strain for the analysed shapes of the bending form

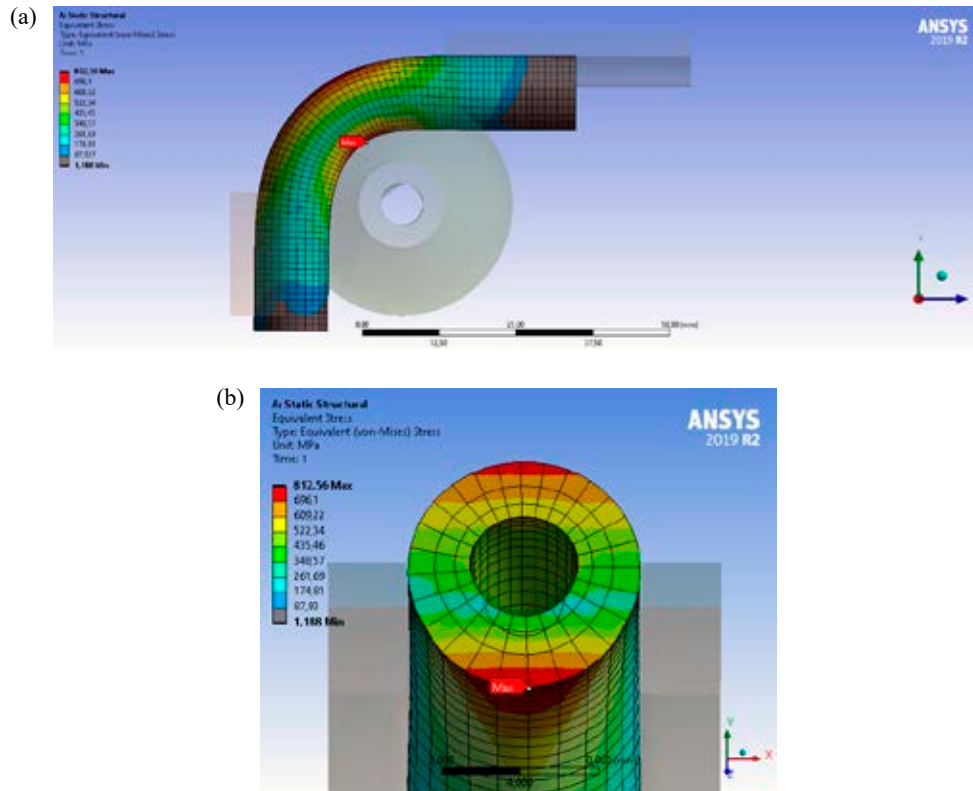| Bending form shape	Parameter			
	Stress		Strain	
	σ tension [MPa]	σ compression [MPa]	ε tension [–]	ε compression [–]
Circular	733.8	783	0.288	0.313
Oval	707.8	791.4	0.274	0.315
Trapezoidal	741.8	812.6	0.293	0.331

Figure 16. (a) Side view of the Von Mises stress distribution in a bend and (b) trapezoidal profile bending form of the von Mises stress distribution in the cross-section of a bending pipe
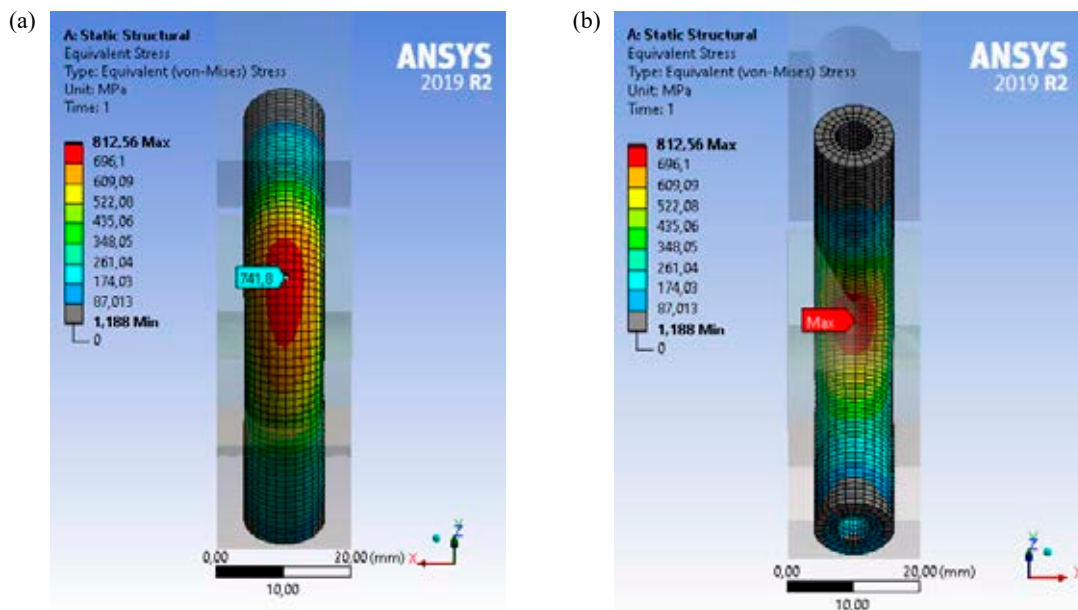

Figure 17. Distribution of the von Mises stress occurring in the (a) outer tensile layer of the bending pipe and (b) inner compression layer of a bending pipe

The results presented in Table 3 are very similar. The difference between the third and the first shape is only 3.6 % for the von Mises stress, and a 5.4 % difference is seen for the plastic strain.

Analysing these outcomes, it can be concluded that the model behaves correctly because the high plastic strain occurred, but not so high as to indicate that the bent material would fail. It can, therefore, be concluded that the results are correct, while the resulting ovalisation value of the cross-section should be used as a criterion for the suitability of the presented bending form.
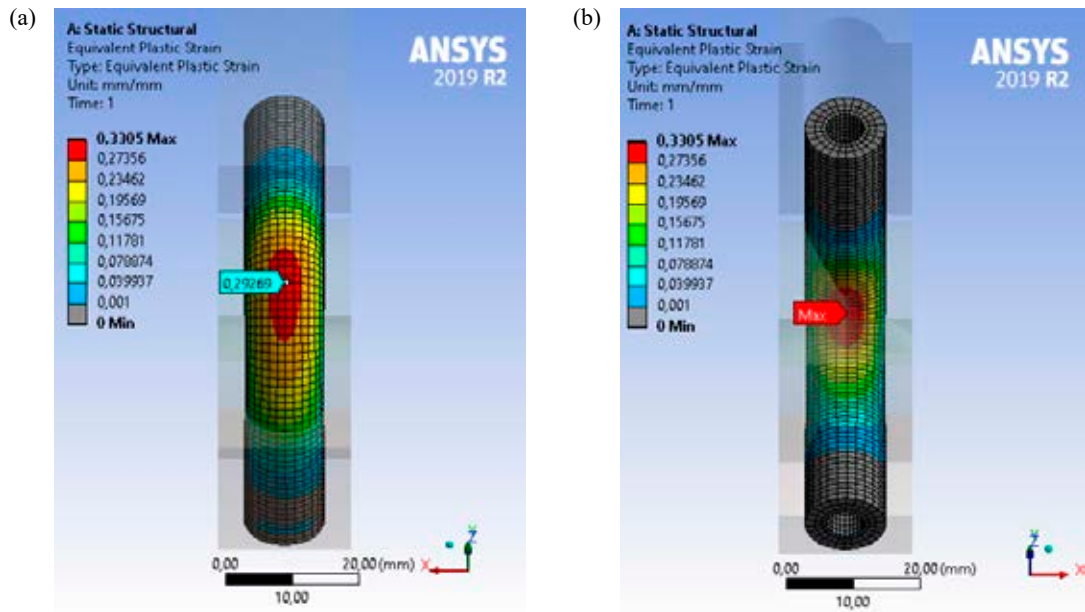
Figure 18. Distribution of plastic strain occurring in the (a) outer tensile layer of a bending pipe and (b) inner compression layer of a bending pipe
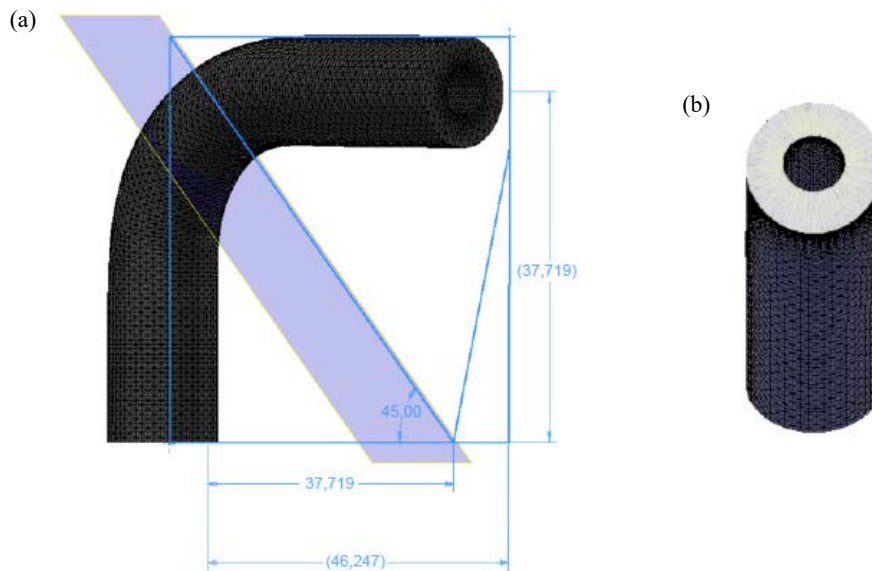

Figure 19. (a) Graphical interpretation of the determination of the ovality-assessed cross-section and (b) view of the ovality-assessed cross-section

Based on the simulation results, the deformed finite element mesh can be exported in *.STL format within the CAD software. To perform a comparative analysis, it was necessary to determine the cross-section from which the minimum diameter, maximum diameter and wall thickness values of the tensile and compression layers were obtained. The cross-section was determined based on the overall dimensions of the pipe and the surface located at 45°, as shown in Figure 19(a). In this surface, the cross-section from which the abovementioned parameters were found occurs.

Figure 19(b) presents the cross-section from which the geometrical dimensions values were found and used for an ovalisation comparative evaluation.

Figure 20 presents the searched parameters adopted to assess the ovalisation of the cross-section of the bend, which were, as mentioned earlier, the maximum cross-section diameter D_{max}, minimum cross-section diameter D_{min}, maximum wall thickness g_{max} and minimum wall thickness g_{min}.

The geometrical parameter values used in the ovalisation comparative evaluation of a bending pipe are presented in Table 4.
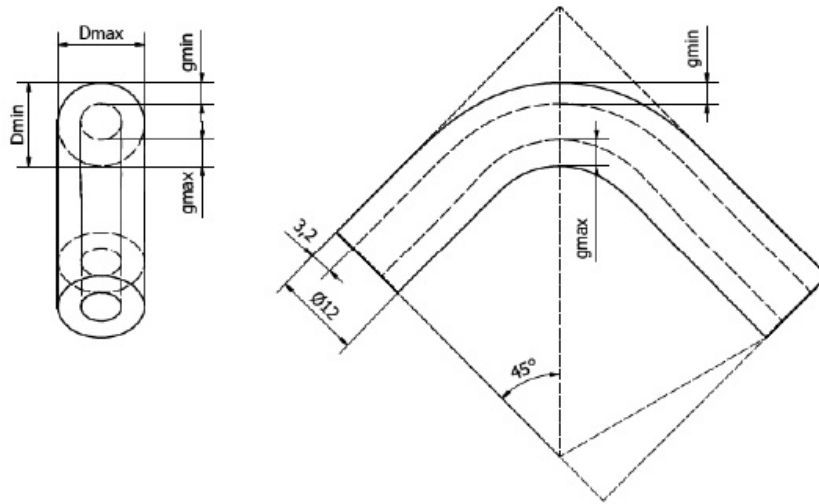
Figure 20. Geometrical parameters used in the ovalisation comparative evaluation of a bending pipe

Table 4. Geometrical parameters used in the ovalisation comparative evaluation of a bending pipe

Bending form shape	Parameters			
	D_{max}	D_{min}	g_{max}	g_{min}
Circular	12	11.45	3.63	2.85
Oval	12.32	11.13	3.62	2.85
Trapezoidal	12	11.67	3.64	2.84

To enable comparative analysis, a comparison was made between the ovalisation and the thinning and wall thickening of the cross-sections obtained by using the bending form with different profiles. The ovalisation expressed as a percentage was determined according to the following formula given in the relevant standard (PN-EN 13480:2021):

$$u = \frac{2\left(d_{o\,max} - d_{o\,min}\right)}{d_{o\,max} + d_{o\,min}} \cdot 100\% \qquad (1)$$

The ovalisation values of the cross-sections of the bend obtained by using a bending form with different profiles, calculated according to equation (1), are presented in Table 5.

Table 5. Ovalisation values of the cross-sections of the bend obtained by using a bending form with different profiles

Bending form shape	Ovalisation value [%]
Circular	4.7
Oval	10.1
Trapezoidal	2.8

For a comprehensive comparison of the effects of using the considered bending form shapes to form the bend, the diagrams shown in Figure 21 can also be used, which show the course of changes in the von Mises stress and plastic strain during the entire pipe bending process using the assumed bending form.
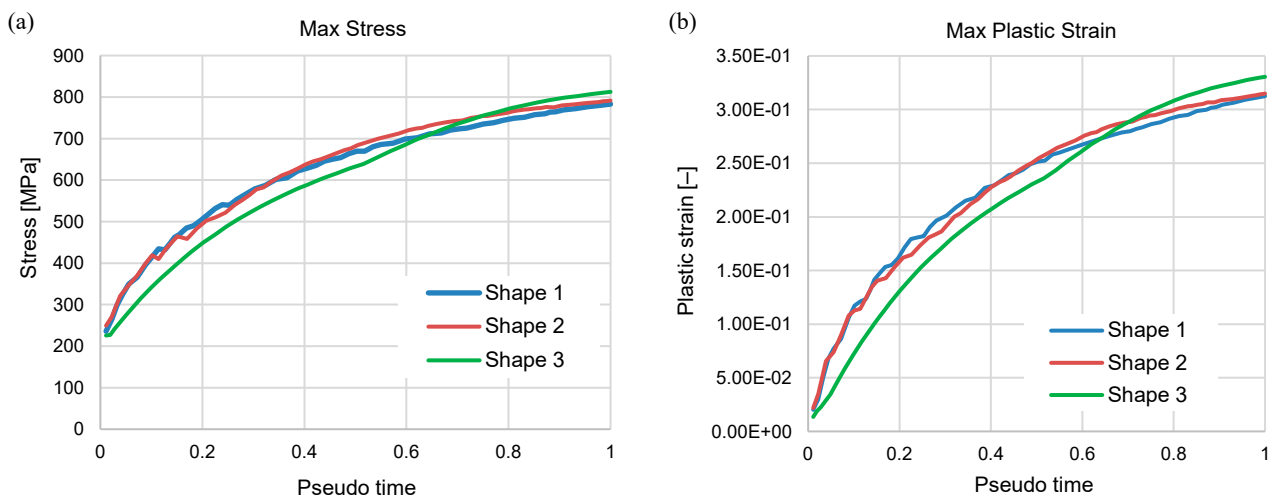

Figure 21. (a) Von Mises stress course and (b) plastic strain course in the analysed cases

Based on the results presented in Figure 21, it can be concluded that, in the first phase of the bending process, the trapezoidal profile is the most favourable from the point of view of minimising stress values and plastic strain. In the second phase of the bending process with a bending angle of 90°, there is an increase in the values of the von Mises stress and plastic strain, which finally results in the highest values of the compared parameters at the end of the bending process.

Conclusions

Based on the analysis of these results, the following conclusions were drawn:
- the shape of the bending form used has a slight influence on the values of the von Mises stress and plastic strain in the bending pipe; however, the shape of the bending form is important due to the minimisation of the ovalisation in the bending pipe;
- for mechanical bending with the bending angle range up to ~50°, the trapezoidal shape is most favourable in terms of the lowest values of the von Mises stress and plastic strain;
- the resulting ovalisation value of the cross-section should be used as a criterion for the suitability of using the adopted bending form shapes to form a bending pipe;
- depending on the shape of the forming segment, the range of variation of the ovalisation values is between 2.8 % and 10.1 %; the minimum value in this range is obtained using a trapezoidal segment.

Considering the above-formulated conclusions, the trapezoidal shape can be considered as the profile by which the final product will be characterised by the most favourable properties in terms of ovalisation of the cross-section of the pipeline section obtained as a result of the mechanical bending process.

References

1. ADAMIEC, P. & DZIUBIŃSKI, J. (2000) Nowoczesne stale na rury i ich spawanie oraz zgrzewanie. *Przegląd Spawalnictwa* 1, pp. 17–22.
2. CAKIROGLU, C., ADEEB, S., CHENG, J.J.R. & SEN, M. (2014) Numerical Analysis of Pressurised Cold Bend Pipes under Bending to Investigate the Transition from Compression to Tension Side Failures. In: Bell, G.R., Card, M.A. (eds). *Structures Congress 2014*, pp. 1990–2001, doi: 10.1061/9780784413357.175.
3. DAMSLET, P.A., BAI, Y., NYSTRØM, P.R. & GUSTAFSSON, C. (1999) Deepwater Pipeline Installation with Plastic Strain. *Proceedings of 18th International Conference on Offshore Mechanics and Arctic Engineering*, July 11–16, 1999, St. John's, Newfoundland, Canada.
4. DOMANOWSKI, P. & NOWAK, B. (2011) Numeryczno-eksperymentalna analiza procesu gięcia rurek z materiału plastycznego. *Przegląd Mechaniczny* 6, pp. 23–28.
5. Euro Inox (2007) *Stainless Steel: Tables of Technical Properties. Materials and Application series, Volume 5*. Euro Inox, Brussels. Available from: https://www.worldstainless.org/Files/issf/non-image-files/PDF/Euro_Inox/Tables_TechnicalProperties_EN.pdf.
6. FUKUDA, N., YATABE, H., KAWAGUCHI, S., WATANABE, T. & MASUDA, T. (2003) Experimental and analytical study of cold bending process for pipelines. *Journal of Offshore Mechanics and Arctic Engineering* 125 (2), pp. 153–157, doi: 10.1115/1.1554701.
7. FUKUDA, N., YATABE, H., MASUDA, T. & TOYODA, M. (2002) Effect of Changes in Tensile Properties Due to Cold Bending on Large Deformation Behavior of High-Grade Cold Bend Pipe. *Proceedings of the 2002 4th International Pipeline Conference. Parts A and B*. Calgary, Alberta, Canada. September 29–October 3, 2002, pp. 363–370, doi: 10.1115/IPC2002-27129.
8. HORIKAWA, H. & NOBUHISA, S. (2009) Bending Deformation of X80 Cold Bend Pipe. Paper presented at the Nineteenth International Offshore and Polar Engineering Conference, Osaka, Japan, July 2009. Available from: https://onepetro.org/ISOPEIOPEC/proceedings-abstract/ISOPE09/All-ISOPE09/7608.
9. JÓŹWIAK, Z. (2011) Ships' ballast water in The Southern Baltic area. *Scientific Journals Maritime University of Szczecin, Zeszyty Naukowe Akademia Morska w Szczecinie* 26 (98), pp. 38–46.
10. KENEDI, P.P., BORGES, L.M.S.A. & VAZ, M.A. (2008) The Interaction Between Pressure and Bending Loadings in PipeCollapse. *V Congresso Nacional de Engenharia Mecânica – CONEM 2008*, Salvador, Bahia.
11. MŁYNARCZAK, A. (2013) Box coolers as an alternative to existing cooling systems. *Scientific Journals Maritime University of Szczecin, Zeszyty Naukowe Akademia Morska w Szczecinie* 36 (108), pp. 131–136.
12. NIEZGODA, T., MAŁACHOWSKI, J. & SZYMCZYK, W. (2004) Rurociągi – modelowanie numeryczne a rzeczywistość. *Przegląd Mechaniczny* 4, pp. 11–18.
13. PACKER, J.A. (2018) *Bending of Hollow Structural Sections*. [Online]. Available from: https://steeltubeinstitute.org/resources/hss-bending-hollow-structural-sections/ [Accessed: February 05, 2024].
14. PŁONECKI, L., WITKOWSKI, G. &, KURP, P. (2018) System synchronizacji napędów urządzenia do laserowo-mechanicznego gięcia rur. *Mechanik* 2, pp. 152–154.
15. PN-EN 13480:2021. *Rurociągi przemysłowe metalowe*.
16. RIAGUSOFF, I.I.T., KENEDI P.P., DE SOUZA, L.F.G. & PACHECO, P.M.C.L. (2010) Modeling of Pipe Cold Bending: A Finite Element Approach. *Conference: VI National Congress of Mechanical Engineering – CONEM 2010*, Campina Granda, Paraiba, Brazil, 18–21 August 2010.
17. SEN, M. & CHENG, R. (2010) Finite Element Analysis of Cold Bend Pipes Under Bending Loads. *Proceedings of the 2010 8th International Pipeline Conference*. Volume 4. Calgary, Alberta, Canada, September 27–October 1, 2010, pp. 257–267, doi: 10.1115/IPC2010-31487.
18. SEN, M., CHENG, J.J.R., MURRAY, D.W. & ZHOU, J. (2006) Mechanical Properties of Cold Bend Pipes. *Proceedings of the 2006 International Pipeline Conference*. Calgary, Alberta, Canada. September 25–29, 2006. pp. 251–257, doi: 10.1115/IPC2006-10436.

19. Sen, M., Cheng, J.J.R. & Zhou, J. (2010) Behavior of cold bend pipes under bending loads. *Journal of Structural Engineering* 137 (5), doi: 10.1061/(ASCE)ST.1943-541X.0000219.

20. Serebrennikov, A. & Serebrennikov, D. (2018) Mathematical model of polyethylene pipe bending stress state. *MEACS 2017, IOP Conf. Series: Materials Science and Engineering 327*, doi: 10.1088/1757-899X/327/4/042099.

21. Simu Tech Group (2019) *Element Quality Plots in Ansys Workbench*. Computer program.

22. Szewczyk, P. (2017) Nowoczesne materiały i technologie do budowy gazociągów wysokiego ciśnienia oraz rurociągów technologicznych na terenach górniczych. *Nafta-Gaz* 10, pp. 778–783.

23. Śloderbach, Z. (1998) Metody obliczania wyjściowej – początkowej grubości rury przeznaczonej do gięcia. *Przegląd Mechaniczny* 21, pp. 9–12.

24. Śloderbach, Z. & Kaźmierczak, J. (2001) Problemy wymiarowe w obliczeniach procesu gięcia rur metalowych według dyrektyw i norm UE oraz Polski. *Przegląd Mechaniczny* 7–8, pp. 38–43.

25. Thomas, P. (2020) Wybrane maszyny i urządzenia stosowane w procesach gięcia. *Stale, Metale & Nowe Technologie* 5/6, pp. 22–27.

26. Traczyk, W. (2019) Gięcie rur o skomplikowanych kształtach. *Magazyn Przemysłowy* 2, pp. 28–31.

27. Trzepieciński, T. (2016) Maszyny stosowane w procesie gięcia. *Stal, Metale & Nowe Technologie* 3/4, pp. 61–68.

28. Xinwei, W., Jie, X., Minghan, D., Yanhu, Z., Zhenlong, W., Bin, G. & Debin, S. (2021) Finite-elements modeling and simulation of electrically-assisted rotary-draw bending process for 6063 aluminum alloy micro-tube. *Metals* 11 (12), 1956, doi: 10.3390/met11121956.